

Correlation structure of a complex system from its subsystems' perspectives

Sen Li(李森), Yan Wang(王燕), Haiying Wang(王海英), Changgui Gu(顾长贵), and Huijie Yang(杨会杰)
Citation: Chin. Phys. B, 2026, 35 (**7**): 078904. DOI: 10.1088/1674-1056/ae42b7
http://cpb.iphy.ac.cn; http://iopscience.iop.org/cpb

What follows is a list of articles you may be interested in

Evolutionary role of startups and its relevance to the success in the blockchain field based on temporal information networks

Ying Wang(王颖) and Qing Guan(管青)
Chin. Phys. B, 2025, 34 (**8**): 088901. DOI: 10.1088/1674-1056/add247

Algorithm for computing time correlation functions in non-stationary complex dynamic systems

Jiu Zhang(张鹫), Lifu Jin(金立孚), Bo Zheng(郑波), Xiongfei Jiang(蒋雄飞), Tingting Chen(陈婷婷), Cong Xu(徐匆), and Yanqing Hu(胡延庆)
Chin. Phys. B, 2025, 34 (**3**): 038904. DOI: 10.1088/1674-1056/adb8bd

A kinetic description of the impact of agent competence and psychological factors on investment decision-making

Chunhua Hu(胡春华) and Hongjing Chen(陈弘婧)
Chin. Phys. B, 2023, 32 (**8**): 088901. DOI: 10.1088/1674-1056/accb4a

Advantage of populous countries in the trends of innovation efficiency

Dan-Dan Hu(胡淡淡), Xue-Jin Fang(方学进), and Xiao-Pu Han(韩筱璞)
Chin. Phys. B, 2022, 31 (**6**): 068903. DOI: 10.1088/1674-1056/ac5614

Information flow between stock markets: A Koopman decomposition approach

Semba Sherehe, Huiyun Wan(万慧云), Changgui Gu(顾长贵), and Huijie Yang(杨会杰)
Chin. Phys. B, 2022, 31 (**1**): 018902. DOI: 10.1088/1674-1056/ac16c9

Correlation structure of a complex system from its subsystems' perspectives

Sen Li(李森), Yan Wang(王燕), Haiying Wang(王海英), Changgui Gu(顾长贵), and Huijie Yang(杨会杰)[†]

Department of Systems Science, University of Shanghai for Science and Technology, Shanghai 200093, *China*

(Received 21 November 2025; revised manuscript received 28 January 2026; accepted manuscript online 6 February 2026)

Detecting the correlation between records is a basic task in data science. Today, researchers try to estimate it from an objective perspective; i.e., they try to remain outside the investigated system and adopt a set of measures representing all the agents precisely and completely. This enables them to answer the questions, 'how often', 'how many', or 'what is the relationship between variables'. In reality, the researcher is usually an agent in the investigated system; they themselves design the metrics for the system's state to answer the questions of 'how' and 'why'. In other words, the researcher conducts the investigation from a subjective perspective. Inspired by qualitative research in social science, in this paper we propose a scheme for investigating complex systems from a subjective perspective. Technically, one decomposes the researcher's output time series into intrinsic mode functions that represent their specific features. Projecting all the agents' time series onto the phase space spanned by this set of specific features, one obtains the coordinates of the agents, from which a similarity network is constructed. The properties of this network are then used to produce a portrait of the system's correlation from the researcher's perspective. As typical examples, we investigate three theoretical models, including the Lorenz system, the Rössler system, and their coupled systems. Although Takens's theorem implies that different variables should be equivalent in reconstructing the dynamical behaviors, we find significant differences between them. We also investigate a financial system composed of 22 stock markets, one crude oil market, and one gold market. The similarity networks for markets distributed across the USA, Europe, and China turn out to be largely homogeneous and dominated by star patterns, while those corresponding to markets distributed across Russia, Brazil, India, and South Africa behave inhomogeneously and are dominated by cluster patterns.

Keywords: correlation structure, subsystems' perspective, investigation from a subjective perspective

PACS: 89.65.Gh, 64.60.aq, 11.15.Me

DOI: 10.1088/1674-1056/ae42b7 **CSTR:** 32038.14.CPB.ae42b7

1. Introduction

A complex system is composed of agents networked by their relationships. This network, the agents' intrinsic dynamics, and the environment cooperatively determine the system's dynamical process. The correlation pattern in the trajectory (output multivariate time series) provides us with information about the underlying dynamical mechanisms and is a powerful tool used for evaluation, regulation, and control.

Different methods have been designed to reveal the multiple features of correlation. In the temporal dimension, correlation within a single time series measures the dependence of the present state on previous states, which is currently detected using the autocorrelation coefficient,[1] the autoregression model,[2] detrended fluctuation analysis,[3] diffusion entropy,[4] and their variants. In the spatial dimension, correlation reveals the interdependence between different variables. The Pearson cross-correlation coefficient[1] and detrended cross-correlation analysis[5] are usually adopted to expose the linear dependence between two variables. The mutual entropy,[6] i.e., the difference between the entropy calculated with the joint probability distribution for a pair of variables and the sum of the entropies calculated from the separate probability distributions of the two variables, successfully exposes the nonlinear dependence between the pair of variables. Causality detection methods such as convergent cross-mapping,[7] time-delay stability,[8] and transfer entropy[9] give us the asymmetrical behavior of interdependence, revealing the causal/influential relationship between one variable and another. Redundancy, defined by means of dimension-reducing algorithms such as principal component analysis[10] and classical correlation analysis,[11,12] is widely adopted to measure the integrated dependence between multiple variables. In the component dimension, a single time series is decomposed into multiple components, the interdependence of which shows us the structure of component correlation.[13] Several concepts, including the structure of causality,[14] pattern dependence,[15] and the graphlet transition matrix,[16–18] have been proposed to reveal the detailed structure of correlation, which is merged into scalar quantities in the shared statistical procedure.

The concepts mentioned above provide a multidimensional picture of correlation in time series, but they are all designed from an objective perspective. As observers outside the investigated system, researchers have a limited and conse-

[†]Corresponding author. E-mail: hjyang@ustc.edu.cn; hjyang@usst.edu.cn

© 2026 Chinese Physical Society and IOP Publishing Ltd. All rights, including for text and data mining, AI training, and similar technologies, are reserved.

quently negligible influence on the system. Researchers have exact knowledge of the variables spanning the phase space in which the system's state is precisely defined. Using a set of metrics for the variables, researchers can accurately record or collect the system's state. Finally, researchers extract the correlation in the system from the numerical data, answering questions like 'how often', 'how many', or 'what is the relationship between variables,' and making an objective decision. This kind of investigation, which operates from an objective perspective, is classified as quantitative research.

In reality, researchers are usually among the agents participating in the structural formation and the dynamical process of the system. They have limited or incomplete knowledge about the other agents, e.g., the variables and the corresponding metrics required to represent the agents' states. They cannot, or are forbidden to, record or collect the agents' trajectories. They must define a set of metrics to obtain representations of the other agents' states from their couplings with them and subsequently construct the trajectory of the whole system from their own perspective. Based on their analysis of this trajectory, a subjective decision is made. In this case, an investigation cannot be conducted from an objective perspective.

What is more, people may sometimes be interested in a deep and detailed understanding of the complexity and nuance of human behavior, social phenomena, or cultural contexts, typically asking the questions 'how' and 'why.' The answers to these questions are stored in the participants' experiences, meanings, perspectives, and processes.[19–21] This approach requires the researchers to treat themselves as an instrument, i.e., all observations, interpretations, and analyses are filtered through their personal lens. This kind of investigation is called qualitative research, which is widely adopted in diverse research fields such as sociology, education, healthcare, and business.

Herein, we cite two typical examples. The first one is from finance. In a stock market, all the investors are interested in specific information that depends strongly on the behaviors of the stocks in their hands and their channels. The investors try to construct a picture of the market by using their own data, upon which a decision is made. The second example is drawn from ecology. Let us consider an ecological system where there are food chains such as grass→field mouse→hawk, grass→rabbit→hawk, grass→locust→sparrow→hawk, and grass→antelope→wolf. For an individual in this system, say the rabbit, its behavior depends on and is formed in turn by the grass, the hawk, the field mouse who share the prey and predator with it, and its population. From the viewpoints of the different kinds of animals, the pictures of the same ecological system are completely different.

In the examples above, each agent preserves the sensitive components of received signals to construct a picture of the system, while the nonsensitive components of the received signals are filtered out or regarded as background, i.e., it is the subjective perceptions, evaluations, and decisions of the individuals that dominate the structure and evolution of the system. In investigations that take place from an objective perspective, the relationships between agents are constructed from the specific behaviors of the couplings between the agents and then abstracted to determine the 'presence' or 'absence' of the linkages, where the detailed physical implications and the resulting rich information about the system are lost.

Accordingly, in this work, we propose a concept called investigation from a subjective perspective (ISP). The key idea is to let each researcher (an agent in the system) define a set of metrics according to their specific features, in the phase space spanned by which all the agents are represented by their mappings to the metrics (phase points). Technically, we decompose the time series for the researcher into intrinsic modes. For every agent, a linear regression model is constructed to explain the data using the intrinsic modes, where the set of regression coefficients is a point in the phase space spanned by the intrinsic modes. The network constructed by means of the distances between the phase points for all agents gives us a picture of the system's structure from the researcher's perspective.

As an illustration of the ISP, we investigate the Lorenz system, the Rössler system, and their coupled system. The similarity networks constructed from the perspectives of the variables have significantly different topological structures, although Takens's theorem tells us that the manifolds formed by their trajectories are equivalent to each other. We also consider an empirical system composed of twenty-four markets, encompassing twenty-two stock markets and two key commodities. The similarity networks from the perspectives of the markets in the USA, Europe, and China are homogeneous, and star patterns dominate their topological structures, providing rich information about the whole system. In contrast, the similarity networks from the perspectives of the markets in Russia, Brazil, India, and South Africa are inhomogeneous; their topological structures are dominated by cluster patterns, providing poor information about the whole system.

As a note, the ISP is different from the ego-net approach,[22–24] where the behavior of a specific node is represented by the pattern formed by it and its neighbors, but the whole network is constructed from an objective perspective.

Section 2 introduces the concept of ISP and the procedure used for its calculation. The results for typical examples are reported in Section 3 and summarized in Section 4.

2. The concept of ISP

Let us consider a complex system with a total of N agents, the trajectories of which, denoted by $X_m, m = 1,2,\ldots,N$, form a multivariate time series of length T:

$$(X_1, X_2, \ldots, X_N) = \begin{pmatrix} x_{11}, x_{12}, \ldots, x_{1N} \\ x_{21}, x_{22}, \ldots, x_{2N} \\ \vdots \\ x_{T1}, x_{T2}, \ldots, x_{TN} \end{pmatrix}. \tag{1}$$

We assume the trajectories have been normalized, i.e., the means and standard deviations are zero and one, respectively.

2.1. Phase space

The first step is to construct a phase space to represent the states of all the agents. In this phase space, the researcher's state should be described precisely, and changes in the state can be distinguished with high precision. Hence, a natural candidate is the space spanned by a set of specific features of the researcher. Different methods can be adopted, such as Fourier transformation, wavelet transformation, principal component decomposition, and classical cross-correlation. If the researcher is an agent with multiple elements, the variables corresponding to the researcher are a natural choice.

In this work, the intrinsic mode functions (IMFs) for the researcher are found by means of ensemble empirical mode decomposition.[25,26] In each IMF, the number of zero crossings is identical to or differs by one from the number of extrema, and for any data point, the average of the envelopes formed by the local maxima and the local minima is zero. Without loss of generality, let us illustrate the procedure using the first time series X_1, i.e., taking the first agent as the researcher. Let the IMFs for X_1 be denoted by $\mathrm{IMF}_1, \mathrm{IMF}_2, \ldots, \mathrm{IMF}_{K^0}$; we now have

$$X_1 = \sum_{k=1}^{K^0} IMF_k + \xi, \tag{2}$$

where ξ is the residual series. Herein, we define the energies of the IMFs as

$$E_k = \sum_{t=1}^{T} [\mathrm{IMF}_k(t)]^2, \quad k = 1,2,\ldots,K^0, \tag{3}$$

i.e., the energy for a specific IMF is the sum of the squares of all its entities. We further assume the IMFs have been ranked in descending order of energy, $E_1 \geq E_2 > \cdots \geq E_{K^0}$. The set of specific features is chosen to be

$$V \equiv \begin{pmatrix} V_1 \\ V_2 \\ \vdots \\ V_K \end{pmatrix} \equiv \begin{pmatrix} \dfrac{\mathrm{IMF}_1}{E_1} \\ \dfrac{\mathrm{IMF}_2}{E_2} \\ \vdots \\ \dfrac{\mathrm{IMF}_K}{E_K} \end{pmatrix}. \tag{4}$$

To determine the number of specific features K, let us define a relative contribution ratio, $R(J) = \frac{\sum_{k=1}^{J} E_k}{\sum_{k=1}^{K^0} E_k}$. Here, K simultaneously satisfies the conditions $R(K) \geq 0.9$ and $R(K-1) < 0.9$.

To represent the agents in the phase space, let us construct a linear model to explain the agents with V,

$$X_n = \beta_{n0} + \sum_{k=1}^{K} \beta_{nk} V_k + \varepsilon_n, \quad n = 1,2,\ldots,N, \tag{5}$$

where ε_n is the noise vector with a size of $T \times 1$, and β_{n0} is a trivial explanatory variable (constant). Taking the regression coefficients β_{nk}, $k = 1,2,\ldots,K$ as the coordinate values in their corresponding dimensions (IMFs), the set $(\beta_{n1}, \beta_{n2}, \ldots, \beta_{nK})$ is a phase point in the phase space spanned by the IMFs, representing the state of the nth agent. Obviously, the state of the observer is $(E_1, E_2, \ldots, E_K)$. Herein, the constant series corresponding to β_{n0} and the residual series ξ are not considered to be characteristics of the observer.

Denoting the Euclidean distance between the mth and nth agents by d^1_{mn}, the distances between all pairs of agents form an original distance matrix D^{01}, i.e.,

$$\begin{aligned} D^{01} &\equiv \left\{ d^1_{mn}, m, n = 1,2,\ldots,N \right\}, \\ d^1_{mn} &= \sqrt{\textstyle\sum_{k=1}^{K} (\beta_{mk} - \beta_{nk})^2}. \end{aligned} \tag{6}$$

Selecting the agents numbered $1,2,\ldots,N$ as researchers, an analogous procedure leads to their corresponding original distance matrices, $D^{01}, D^{02}, \ldots, D^{0N}$, giving us portraits of the system from the agents' perspectives.

2.2. An N-dimensional portrait

Some strategies can be used to filter out noise or insignificant relationships in the original distance matrices to expose the dominant patterns within the set of resulting distance networks. For example, one can simply assign a distance threshold and preserve only the relationships with distances smaller than the threshold. Alternatively, for each agent, we preserve only a specified number of the smallest-distance relationships. If we rank the entities in the original distance matrices in ascending order, the part of the curve for the smallest distances usually obeys a specific law different from that of the other parts. The crossover is accordingly chosen to be the threshold, which is adopted in this work.

Denoting the threshold distance by d^*, the distance networks $A^d = \left\{ A^{d1}, A^{d2}, \ldots, A^{dN} \right\}$ are defined as

$$A^{dn}_{mk} \equiv \frac{d^n_{mk}}{d^*} \times H(d^* - d^n_{mk}), \quad n, m, k = 1,2,\ldots,N, \tag{7}$$

where d^n_{mk} is the entity at the mth row and nth column in the original distance matrix D^{0n}, and $H(\cdot)$ equals 1 and 0 when the

dummy is ≥ 0 and < 0, respectively. This set of distance matrices gives us an N-dimensional portrait of the system (a multiplex network). For visual convenience in drawing this portrait, we define a set of similarity networks $A^s = \{A^{s1}, A^{s2}, \ldots, A^{sN}\}$, the entities in which read

$$A^{sn}_{mk} = 1 - A^{dn}_{mk}, \quad n,m,k = 1,2,\ldots,N. \tag{8}$$

It should be noted that a large similarity between an agent and the researcher definitely implies that the specific features of the researcher can explain most or even all of the agent's behavior. However, for two agents other than the researcher, a large similarity does not necessarily imply that they share behaviors that can be represented by the researcher's specific features. If the researcher's specific features have low explanatory power for both agents, the coordinates for the two agents will lie near the origin in phase space, which also implies a large similarity. From the perspective of the researcher, they are classified into the 'unexplainable' class. Therefore, if two agents have a large similarity to each other but both have weak similarities to the researcher, that large similarity arises from their belonging to the 'unexplainable' class.

2.3. Properties of the N-dimensional portrait

The characteristics of the constructed networks are displayed with several topological properties, which are illustrated herein with the network from the nth agent's perspective.

Average weight per node This measure is a global evaluation of the connection strength, showing us to what extent the specific features of node n (the researcher) can represent the behaviors of all the agents. Denoting this measure by WPN, we have

$$\mathrm{WPN}(n) = \frac{1}{2N} \sum_{m\neq k=1,2,\ldots,N} A^{sn}_{mk}. \tag{9}$$

Clique-star For node i, one extracts the ego-net. Let $\mathrm{DEG}(i)$ denote the number of its neighbors, and let $\mathrm{EDG}(i)$ denote the number of edges in this local pattern, which can be calculated with

$$\begin{aligned} &\mathrm{DEG}(i) = \textstyle\sum_{m=1}^{N} \delta\left(A^{sn}_{mi}\right), \\ &\mathrm{EDG}(i) = \mathrm{DEG}(i) + \textstyle\sum_{m\neq k=1}^{N} \delta\left(A^{sn}_{mi} \cdot A^{sn}_{ki} \cdot A^{sn}_{mk}\right), \\ &i = 1,2,\ldots,N, \end{aligned} \tag{10}$$

where $\delta(\cdot)$ equals 1 and 0 when the dummy $\neq 0$ and $= 0$, respectively. Generally speaking, there exists a power-law relation

$$\mathrm{EDG}(i) \sim [\mathrm{DEG}(i)]^{\gamma_n}, \quad i = 1,2,\ldots,N. \tag{11}$$

When all the neighbors are disconnected from or connected to each other, we have $\mathrm{EDG}(i) = \mathrm{DEG}(i)$ or $\mathrm{EDG}(i) = \mathrm{DEG}(i) + \mathrm{DEG}(i) \times [\mathrm{DEG}(i) - 1] = [\mathrm{DEG}(i)]^2$, $i = 1,2,\ldots,N$, i.e., $\gamma_n \in [1,2]$. The extreme cases of $\gamma_n = 1$ and 2 imply a star graph and a clique graph, respectively. The scaling exponent γ_n accordingly describes the clustering effect. A larger (smaller) clustering effect implies that the agent and its neighbors share a larger (smaller) subset of the specific features of the researcher.

Heavy vicinity The summation of the edge weights in the ego-net for node i reads

$$\mathrm{SUW}(i) = \sum_{m=1}^{N} A^{sn}_{mi} + \frac{1}{2} \sum_{m\neq k=1}^{N} \delta(A^{sn}_{im} \cdot A^{sn}_{ik}) A^{sn}_{mk}, \tag{12}$$

which usually also satisfies a power law

$$\mathrm{SUW}(i) \sim [\mathrm{EDG}(i)]^{\alpha_n}, \quad i = 1,2,\ldots,N. \tag{13}$$

A larger α_n, i.e., the summation of weights, increases rapidly with the number of edges, implying that there exist some nodes that link strongly with many agents, i.e., they form a group sharing the same features.

Dominant pair In the ego-net for node i, the weights for the edges from node i to its neighbors are generally distributed over a wide range. This inhomogeneity is typically measured with the principal eigenvalue of the adjacency matrix of the ego-net, $\lambda_i^{\max}$, which usually also obeys a power law

$$\lambda_i^{\max} \sim [\mathrm{SUW}(i)]^{\eta_n}, \quad i = 1,2,\ldots,N. \tag{14}$$

A larger η_n implies a much more inhomogeneous distribution of the weights, i.e., there exist some agents that share almost all of their features with node n.

3. Results

The proposed method is first illustrated with three chaotic models. Then it is used to show the correlation structure for a global financial system composed of twenty-four markets, encompassing twenty-two stock markets, one crude oil market (Brent), and one gold market (XAU/USD).

Case I: Lorenz system This dynamical system is composed of three variables x, y, and z, satisfying[27]

$$\begin{aligned} \frac{\mathrm{d}x}{\mathrm{d}t} &= -a(x-y), \\ \frac{\mathrm{d}y}{\mathrm{d}t} &= bx - y - xz, \\ \frac{\mathrm{d}z}{\mathrm{d}t} &= -cz + xy, \end{aligned} \tag{15}$$

where $(a,b,c) = (10,28,8/3)$. A trajectory is generated with the initial state of $(x_0,y_0,z_0) = (12,2,9)$ and the time step 0.01. A total of 2×10^4 time steps are simulated, of which the first 10^4 records are discarded to remove the transient process, resulting in a time series with a length of 10^4 (see Fig. 1(a1)). The three series x,y,z have been normalized separately, as required by the ISP algorithm.

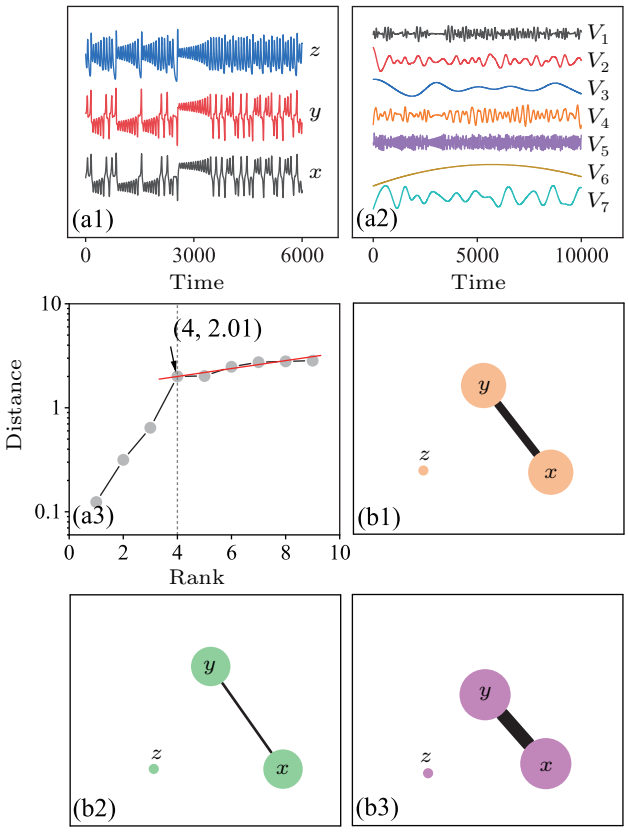


Fig. 1. A portrait of the Lorenz system from multiple perspectives. (a1) Trajectories for x, y, and z (normalized respectively). (a2) Specific features of x, as a typical example. (a3) All the entities in the original distance matrices from the perspectives of x, y, and z, ranked in ascending order. (b1)–(b3) The similarity networks from the perspectives of x, y, and z, respectively.

Selecting x as the researcher, it has seven specific features in total, as shown in Fig. 1(a2), covering a wide range of characteristic periods. The coordinates for x, y, and z in the phase space spanned by this set of specific features, denoted by $V^{\cdot|x} \equiv \left(V^{x|x}, V^{y|x}, V^{z|x}\right)$, read

$$V^{\cdot|x} = \begin{pmatrix} 1.114 & 0.971 & -0.129 \\ 0.955 & 0.858 & 0.083 \\ 0.996 & 0.866 & -0.222 \\ 0.989 & 0.873 & -0.081 \\ 1.020 & 0.902 & 0.001 \\ 0.834 & 0.732 & 0.025 \\ 1.046 & 0.924 & -0.038 \end{pmatrix}. \tag{16}$$

By means of an analogous procedure, the coordinates for x, y, and z from the perspective of y and z, denoted by $V^{\cdot|y} \equiv \left(V^{x|y}, V^{y|y}, V^{z|y}\right)$ and $V^{\cdot|z} \equiv \left(V^{x|z}, V^{y|z}, V^{z|z}\right)$, read

$$V^{\cdot|y} = \begin{pmatrix} 0.621 & 1.242 & 0.013 \\ 0.820 & 0.879 & 0.043 \\ 1.031 & 1.012 & -0.204 \\ 1.046 & 0.984 & -0.114 \\ 1.052 & 0.982 & -0.018 \\ 0.991 & 0.907 & 0.043 \\ 1.254 & 1.167 & -0.023 \end{pmatrix},$$

$$V^{\cdot|z} = \begin{pmatrix} -0.172 & -0.064 & 0.949 \\ 0.101 & 0.047 & 1.004 \\ -0.215 & -0.242 & 1.203 \end{pmatrix}. \tag{17}$$

Figure 1(a3) presents all the values of the entities in D^{0x}, D^{0y}, and D^{0z}, ranked in ascending order. In both of the distance ranges separated by 2.01, the distance increases exponentially, but the exponent corresponding to the former part is significantly larger than that corresponding to the latter one. Accordingly, the selected threshold is $d^* = 2.01$.

Figures 1(b1)–1(b3) depict the topological structures for A^{sx}, A^{sy}, and A^{sz}, respectively. The strong linkages between x and y in the three networks imply that the features of x and y overlap strongly. The features of z have limited overlap with those of x and y. Accordingly, the variables x and y can represent each other with a high degree of correlation. Takens's theorem tells us that the trajectories for x, y, and z each store the complete information for the whole system; thus, the manifolds constructed by embedding them in a high-dimensional phase space are equivalent to the manifold for the whole system. However, our results show that z has features that significantly differ from those of x and y.

Case II: Rössler system This system consists of three variables x, y, and z, with the relationships[28]

$$\begin{aligned} \frac{\mathrm{d}x}{\mathrm{d}t} &= -y - z, \\ \frac{\mathrm{d}y}{\mathrm{d}t} &= x + ay, \\ \frac{\mathrm{d}z}{\mathrm{d}t} &= b + z(x - c), \end{aligned} \tag{18}$$

where the parameters read $(a, b, c) = (0.2, 0.2, 5.7)$. Using initial conditions of $(x_0, y_0, z_0) = (0, 0, 0)$ and a time step of 0.01, 2×10^4 steps are simulated, where the last 10^4 records form the considered trajectory. The series x, y, and z (normalized separately) are depicted in Fig. 2(a1). Selecting x as the researcher, it has only a single specific feature, as shown in Fig. 2(a2). The coordinates for x, y, and z in the phase space spanned by this set of specific features, denoted by $V^{\cdot|x} \equiv \left(V^{x|x}, V^{y|x}, V^{z|x}\right)$, read

$$V^{\cdot|x} = \begin{pmatrix} 1.065 & -0.113 & 0.232 \end{pmatrix}. \tag{19}$$

By means of an analogous procedure, the coordinates for x, y, and z from the perspective of y and z, denoted by $V^{\cdot|y} \equiv \left(V^{x|y}, V^{y|y}, V^{z|y}\right)$ and $V^{\cdot|z} \equiv \left(V^{x|z}, V^{y|z}, V^{z|z}\right)$, read

$$V^{\cdot|y} = \begin{pmatrix} -0.199 & 1.075 & 0.272 \\ -0.111 & 0.946 & -1.224 \end{pmatrix},$$

$$V^{\cdot|z} = \begin{pmatrix} -0.135 & 0.047 & 0.977 \\ 0.407 & 0.219 & 1.064 \\ -0.622 & -0.212 & 0.976 \\ 0.942 & 0.742 & 1.041 \\ 0.543 & 0.338 & 0.834 \\ 0.358 & -0.992 & 1.406 \end{pmatrix}. \tag{20}$$

Figure 2(a3) presents all the values of the entities in D^{0x}, D^{0y}, and D^{0z}, ranked in ascending order. Starting from the distance 1.21, the curve follows an exponential law, while in the

range ≤ 1.21, the curve increases rapidly at the beginning and finally saturates at a constant value. Accordingly, the selected threshold is $d^* = 1.21$.

Figures 2(b1)–2(b3) depict the topological structures for A^{sx}, A^{sy}, and A^{sz}, respectively. From the perspective of x (panel (b1)), there are strong linkages between x and z and between y and z, but an ignorable one between x and y, telling us that in the phase space spanned by x's specific features, the positions of z and y are the closest, those of z and x are intermediate, and those of x and y are the farthest (filtered out by the threshold); these are straightforward deductions from the coordinates in Eq. (19). From the perspectives of y and z (panels (b2) and (b3)), x, y, and z are all isolated. In the coordinates from the perspective of y, as presented in Eq. (20), x is very close to the origin; i.e., the specific features for y cannot represent the dominant behavior of x. The pairwise distances between x, y, and z are large. From the perspective of z, x, y and z share only the behavior corresponding to the 4th IMF, whose coordinates are 0.942, 0.742, and 1.041, respectively. Hence, in the topological structures presented in Figs. 2(b2) and 2(b3), x, y, and z are isolated nodes.

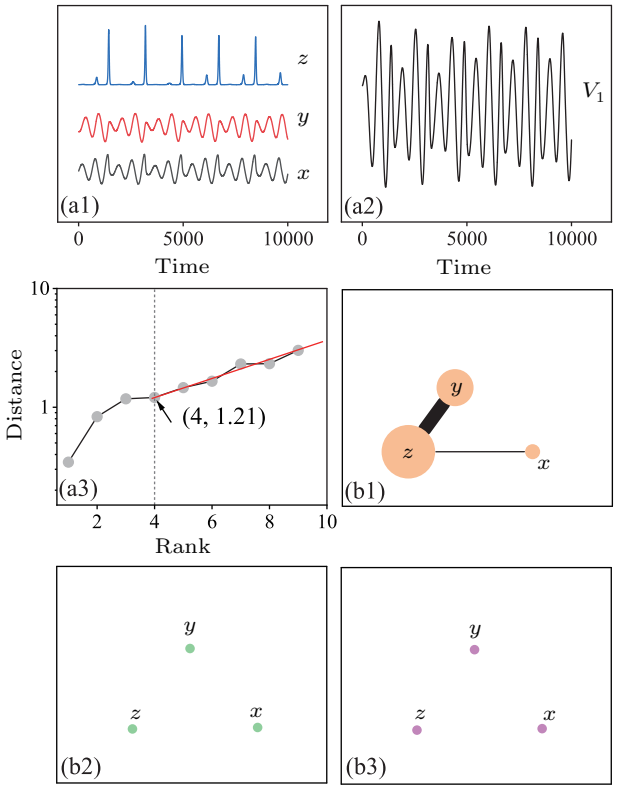


Fig. 2. A portrait of the Rössler system from multiple perspectives. (a1) Trajectories for x, y, and z (normalized respectively). (a2) Specific features of x, as a typical example. (a3) All the entities in the original distance matrices from the perspectives of x, y, and z, ranked in ascending order. (b1)–(b3) The similarity networks from the perspectives of x, y, and z, respectively.

Case III: Coupled Rössler and Lorenz systems The two systems mentioned above are coupled as defined below:[29]

$$\begin{aligned}
\frac{\mathrm{d}x_1}{\mathrm{d}t} &= -6(y_1+z_1),\\
\frac{\mathrm{d}y_1}{\mathrm{d}t} &= 6(x_1+0.2y_1),\\
\frac{\mathrm{d}z_1}{\mathrm{d}t} &= 6(0.2+z_1(x_1-5.7),\\
\frac{\mathrm{d}x_2}{\mathrm{d}t} &= 10(y_2-x_2),\\
\frac{\mathrm{d}y_2}{\mathrm{d}t} &= x_2(28-z_2)-y_2+Cy_1^2,\\
\frac{\mathrm{d}z_2}{\mathrm{d}t} &= x_2y_2-\frac{8}{3}z_2,
\end{aligned} \tag{21}$$

where C is the coupling strength. For the initial conditions of $(x_{10}, y_{10}, z_{10}, x_{20}, y_{20}, z_{20}) = (0.1, 0.1, 0.1, 12, 2, 9)$ and a time step of 0.01, a total of 2×10^4 steps are simulated, where the last 10^4 records form the considered trajectory. Three coupling strengths of $C = 1$, 3, and 8 are chosen to show the differences under weak, normal, and strong couplings; the corresponding normalized trajectories are presented in Figs. 3(a1), 3(b1), and 3(c1), where only the initial 6×10^3 points are shown for visual convenience.

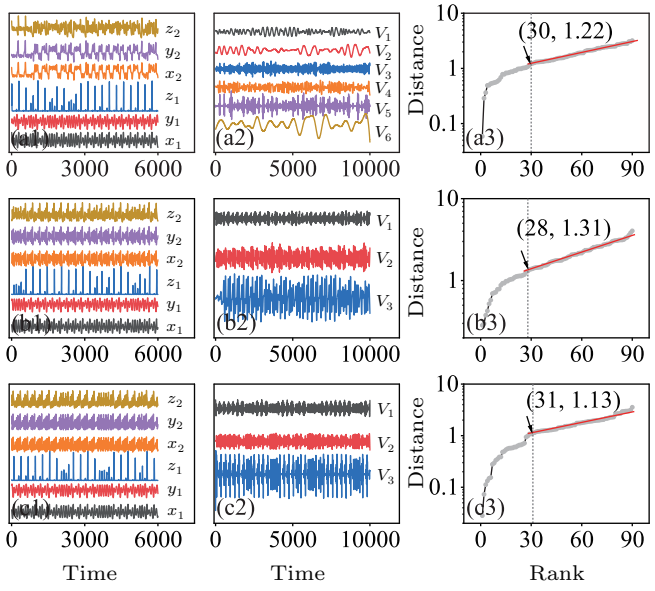


Fig. 3. Trajectories and distance thresholds for the coupled Rössler and Lorenz systems. (a1), (b1), (c1) Normalized trajectories for x_1, y_1, z_1, x_2, y_2 and z_2 with $C = 1$, 3, 8, respectively. A view covering a total of 6×10^3 points is drawn for visual convenience. (a2), (b2), (c2) Intrinsic mode functions used to represent the specific features of the researcher y_2 for $C = 1$, 3, 8, respectively. The entities for the original distance matrices from all perspectives are ranked in ascending order in (a3), (b3), and (c3) for $C = 1$, 3, and 8, respectively.

For a coupling strength of $C = 1$, selecting y_2 as the researcher, there is a total of 6 specific features, as shown in Fig. 3(a2), covering a wide range of characteristic periods. The coordinates for x_1, y_1, z_1, x_2, y_2 and z_2 in the phase space spanned by this set of specific features, denoted by $V^{\cdot|y_2}(C=1) \equiv \left(V^{x_1|y_2}, V^{y_1|y_2}, V^{z_1|y_2}, V^{x_2|y_2}, V^{y_2|y_2}, V^{z_2|y_2}\right)|_{C=1}$, read

$$V^{\cdot|y_2}(C=1)$$

$$= \begin{pmatrix} -0.069 & 0.443 & -0.232 & 0.319 & 1.018 & 0.093 \\ 0.338 & -0.506 & -0.348 & 0.606 & 0.994 & -0.321 \\ 0.157 & -0.777 & -0.217 & 0.831 & 0.997 & 0.251 \\ -0.119 & 0.090 & 0.064 & 1.065 & 1.004 & 0.493 \\ 0.024 & -0.119 & 0.089 & 1.054 & 0.978 & 0.271 \\ 0.043 & -0.064 & -0.026 & 1.280 & 1.189 & 0.384 \end{pmatrix}. \quad (22)$$

For the coupling strengths $C = 3$ and $C = 8$, selecting y_2 as the researcher, the specific features are shown in Figs. 3(b2) and 3(c2). The coordinates for $x_1, y_1, z_1, x_2, y_2, z_2$ in the phase spaces spanned by them, denoted with $V^{\cdot|y_2}(C = 3)$ and $V^{\cdot|y_2}(C = 8)$, read

$$V^{\cdot|y_2}(C = 3)$$
$$= \begin{pmatrix} -0.083 & 0.143 & -0.081 & 0.481 & 1.051 & -0.184 \\ -0.125 & -0.958 & -0.517 & 0.991 & 0.999 & -0.015 \\ -1.509 & -0.766 & -1.676 & 1.212 & 1.118 & -0.235 \end{pmatrix}, \quad (23)$$

$$V^{\cdot|y_2}(C = 8)$$
$$= \begin{pmatrix} 0.315 & -0.022 & -0.153 & -0.077 & 1.028 & -0.241 \\ -0.053 & 0.060 & 0.182 & 0.543 & 0.922 & -0.100 \\ -0.151 & -0.295 & -0.508 & 0.897 & 1.118 & -0.019 \end{pmatrix}. \quad (24)$$

All the entities in D^{0x_1}, D^{0y_1}, D^{0z_1}, D^{0x_2}, D^{0y_2}, and D^{0z_2} are ranked in ascending order. The distance turns out to increase exponentially in the range > 1.22, which is completely different from the behavior observed in the range ≤ 1.22 (see Fig. 3(a3)). Hence, the threshold selected for the case $C = 1$ is $d^* = 1.22$. Using an analogous procedure, the distance thresholds for the cases $C = 3$ and $C = 8$ are determined to be $d^* = 1.31$ (see Fig. 3(b3)) and 1.13 (see Fig. 3(c3)), respectively.

The constructed similarity networks corresponding to the researchers $x_1, y_1, z_1, x_2, y_2, z_2$ for the cases of $C = 1$, 3, and 8 are depicted in panels (a1)–(a6), (b1)–(b6), and (c1)–(c6) in Fig. 4. The similarity networks constructed by different researchers have different structures. For instance, when y_2 is chosen as the researcher, in the case of weak coupling with $C = 1$ (see panel (a5)), the coordinates for x_2 and y_2 are $(0.319, 0.606, 0.831, 1.065, 1.054, 1.280)^\dagger$ and $(1.018, 0.994, 0.997, 1.004, 0.978, 1.189)^\dagger$ (see Eq. (22)); in other words, the coordinates corresponding to the 4th, 5th, and 6th specific features are large and almost identical. Therefore, x_2 and y_2 are strongly linked. The linkage between x_1 and z_1 is due mainly to the fact that they share an absence of the 4th, 5th, and 6th specific features. When the coupling strength becomes normal ($C = 3$; see Fig. 4(b5)), the coordinates for x_2 and y_2 are $(0.481, 0.991, 1.212)^\dagger$ and $(1.051, 0.999, 1.118)^\dagger$ (see Eq. (23)); thus, the coordinates for the 2nd and 3rd specific features are large and almost identical, meaning that x_2 and y_2 are strongly linked. The strong linkage between x_1 and z_1 is due to the fact that they share the absence of the first feature and the near agreement of their large (negative) coordinates for the third feature. When C becomes large ($C = 8$; see Fig. 4(c5)), x_1, y_1, z_1, and z_2 are strongly linked to each other, forming a tightly clustered graph. From Eq. (24), one can find that the coordinates for these four series are all small, except for the third one (for z_1 (-0.508)), with the absolute values of five of them ≤ 0.1. Hence, this tightly clustered structure arises because the y_2 features are a poor representation of the four series.

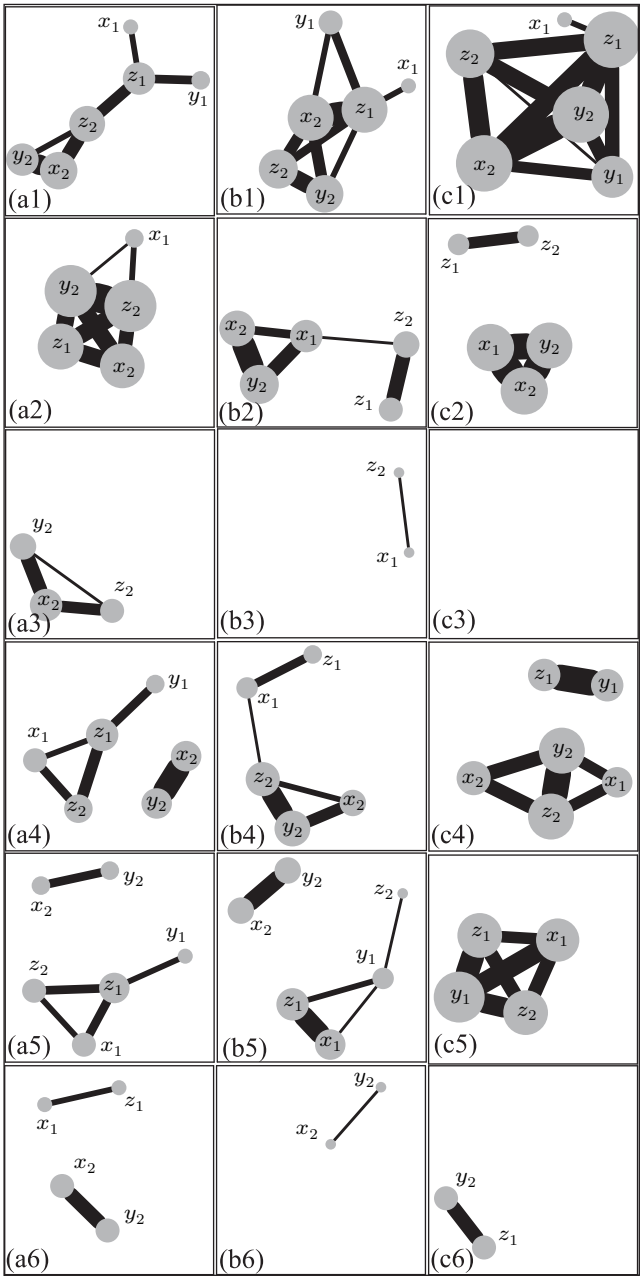


Fig. 4. Similarity networks for the coupled Rössler and Lorenz systems. The panels are numbered (uv), where the symbols $u =$ a, b, and c correspond to coupling strengths of $C = 1$, 3, and 8, and $v = 1, 2, 3, 4, 5$ and 6 correspond to the variables x_1, y_1, z_1, x_2, y_2 and z_2 that are chosen to be researchers, respectively. As an example, panel (a6) shows the similarity network from the perspective of z_2 when the coupling strength is $C = 1$.

Case IV: An empirical case As a typical example of an empirical case, we consider a financial system consisting of 22 stock indices, one crude oil price, and one gold price,[30,31] as listed in Table 1. The time series are separated into three periods corresponding to before, during, and after COVID-19,[32]

covering the durations from January 1, 2017 to December 31, 2019; from January 1, 2020 to December 31, 2022; and from January 1, 2023 to October 25, 2025, respectively. We preserve only the daily records for which all the records for the 24 markets are present. A logarithmic return is adopted; i.e., from the original time series for every specific market with length T, $p_1, p_2, \ldots, p_T$, we convert it into a return series, $R_{t-1} = \ln(p_t/p_{t-1}), t = 2, 3, \ldots, T$.

Table 1. List of 22 stock market indices, one crude oil price, and one gold price, including their IDs and abbreviations.

ID	Market name	Abbreviation
1	Shanghai Composite Index	SSEC
2	Hang Seng Index	HSI
3	Dow Jones Industrial Average	DJI
4	German DAX Index (DAX 30)	DE40
5	CAC 40 Index	FCHI
6	FTSE 100 Index	UK100
7	Nikkei 225 Stock Average	JP225
8	Ibovespa Index	IBOV
9	Taiwan Weighted Index	TWII
10	S&P BSE Sensex 30	BSESN
11	Korea Composite Stock Price Index	KS50
12	RTS Index	IRTS
13	FTSE/JSE Africa Top 40 Index	JTOPI
14	S&P/ASX 200 Index	AXJO
15	Qatar Stock Exchange Index	QSI
16	S&P 500 Index	US500
17	NASDAQ Composite Index	IXIC
18	EURO STOXX 50 Index	STOXX50
19	Tadawul All Share Index	TASI
20	Shenzhen Component Index	SZI
21	Straits Times Index	STI
22	Indonesia Composite Index	JKSE
23	Crude Oil Prices: Brent–Europe	Brent
24	Gold spot price	XAU/USD

The 24 markets are distributed over the whole world, forming a global financial system, but we separate the periods according to the specific stages of the pandemic in China. The first reason is that COVID-19 caused a serious shock and persistently influenced international society, economics, and trade. The influence of the pandemic on the global financial system is an interesting problem. The second reason is that the Chinese government was among the first to implement strict prevention and control measures; i.e., the duration of prevention and control conducted by the Chinese government was the longest, overlapping all the others across the world.

To show why the COVID-19 pandemic period is identified as the three years from January 2020 to December 2022, we list the time nodes for this pandemic in China. The first patient suffering from this disease in China was reported[33] with an infection date traced back to December 1, 2019. On December 31, 2019, the number of patients increased to a total of 27, which led to a series of actions, including the successive activations of level-II and level-I emergency responses on January 6, 2020, and on January 15, 2020. On January 20, 2020, COVID-19 was identified as a 'category A infectious disease' by the Chinese government. Nationwide, the numbers of patients and the numbers of persons who died from this disease reached 11791 and 259 on January 31, 2020, and increased rapidly to 20438 and 425 on February 3, 2020, respectively. The outbreak of this pandemic led to a series of strictly implemented prevention and control policies and measures and their variants. On December 7, 2022, the accumulated number of patients and the number of people who died from this disease were $N_{\text{patients}} = 354000$ and $N_{\text{deaths}} = 5235$, respectively; thus, the death rate $\frac{N_{\text{deaths}}}{N_{\text{patients}}}$ was reduced to $\frac{5235}{354000} = 1.48\%$. On January 8, 2023, the Chinese government adjusted the 'category A infectious disease' to a 'category B infectious disease'. Prevention and control measures were subsequently revoked. On the same day, in Shanghai, one of the most developed cities with the highest population, the free nucleic acid testing service was canceled.

Figure 5 presents all the distances from the perspectives of each market before (panel (a)), during (panel (b)), and after (panel (c)) COVID-19. The positions of the crossovers, namely, 0.21, 0.19, and 0.21, are chosen as the values of the distance threshold d^*, respectively.

In Fig. 5(d), we show the average weights for the similarity networks from each market's perspective. The upper/lower red-dotted horizontal lines indicate the mean plus/minus 1.5 times the standard deviation of the average weights. The markets whose average weights are above the upper red-dotted line include the market with ID number 12 from Russia during and after COVID-19, two with ID numbers 14 from Australia and 15 from Qatar during COVID-19, the market with ID number 20 from Mainland China, and the market with ID number 24 (the gold market).

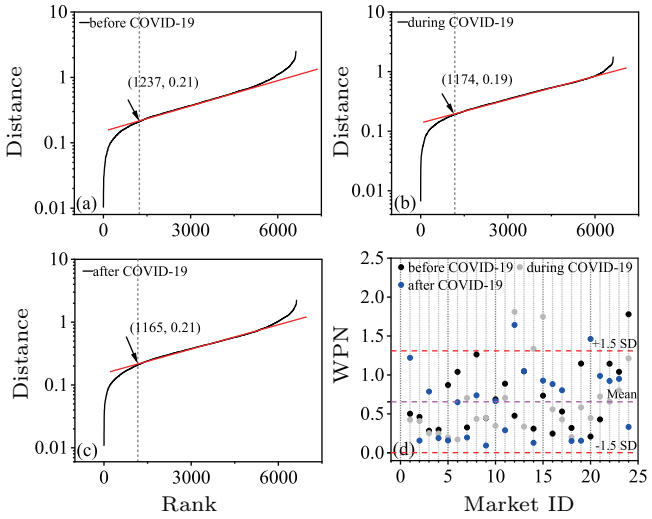


Fig. 5. The empirical case of a financial system composed of 24 agents listed in Table 1. (a)–(c) Distances between agents from each agent's perspective, ranked in ascending order, for the periods before, during, and after COVID-19, respectively. (d) Average weights for each market.

Table 2. The scaling exponents γ_n, α_n, and η_n for the constructed similarity networks for the empirical financial system. In each column, the largest and the smallest exponents are highlighted in red and blue, respectively. In the 'before, during, and after' COVID-19 periods, the rows that are not correlated with COVID-19 are highlighted in gray.

	γ_n			α_n			η_n		
ID	Before	During	After	Before	During	After	Before	During	After
1	1.58	1.65	1.62	1.48	1.33	0.95	0.76	0.73	0.54
2	1.50	1.50	1.41	0.91	1.45	1.43	0.61	0.79	0.83
3	1.51	1.51	1.55	1.09	1.37	1.31	0.75	0.75	0.70
4	1.42	1.48	1.34	1.07	0.87	0.91	0.69	0.74	0.79
5	1.64	1.35	1.29	1.03	0.56	1.72	0.57	0.64	0.82
6	1.63	1.39	1.53	1.20	1.01	1.28	0.69	0.73	0.65
7	1.54	1.74	1.40	1.37	0.95	0.88	0.83	0.57	0.74
8	1.67	1.50	1.72	0.89	1.18	1.27	0.48	0.65	0.68
9	1.56	1.67	1.22	1.59	1.48	0.53	0.81	0.77	0.92
10	1.58	1.56	1.63	1.16	1.55	1.16	0.65	0.78	0.64
11	1.60	1.65	1.42	1.04	1.24	0.85	0.60	0.71	0.62
12	1.61	1.87	1.65	1.20	1.11	0.96	0.65	0.65	0.45
13	1.64	1.64	1.64	1.93	1.31	1.18	0.80	0.77	0.67
14	1.40	1.75	1.29	1.20	0.94	1.53	0.77	0.56	0.90
15	1.56	1.79	1.55	1.24	1.41	1.13	0.64	0.72	0.61
16	1.39	1.47	1.72	1.47	1.24	0.99	0.81	0.78	0.57
17	1.55	1.56	1.63	0.87	0.97	1.15	0.65	0.65	0.69
18	1.49	1.35	1.39	1.46	0.68	1.28	0.86	0.78	0.91
19	1.74	1.55	1.42	1.15	1.31	1.65	0.52	0.68	0.91
20	1.51	1.61	1.71	1.29	1.40	1.17	0.80	0.73	0.63
21	1.59	1.63	1.66	1.54	1.18	0.91	0.81	0.65	0.51
22	1.65	1.61	1.54	1.28	1.27	1.06	0.70	0.69	0.58
23	1.69	1.67	1.64	1.18	1.31	1.18	0.64	0.67	0.64
24	1.93	1.62	1.45	1.25	1.02	1.36	0.70	0.54	0.83

The power laws in Eqs. (11), (13), and (14) stand for all the constructed similarity networks, as shown in Fig. 6, including several typical examples of curves from the perspectives of HSI (ID number 2), IBOV (ID number 8), TASI (ID number 19), and XAU/USD (ID number 24) before, during, and after COVID-19. By regressing the curves in the log–log coordinate frame with a linear function, one obtains the scaling exponents, as shown in Table 2.

Before COVID-19, we have $\gamma_n \in [1.39, 1.93]$. The gold spot price (with ID 24) has the largest value of $\gamma_n = 1.93$. The S&P 500 Index (with ID 16), the S&P/ASX 200 Index, and the German DAX Index have the smallest values of $\gamma_n \sim 1.40$. During COVID-19, we have $\gamma_n \in [1.35, 1.87]$. The RTS Index, with an ID number of 12 (from Russia), has the largest value of $\gamma_n = 1.87$, while the smallest value of $\gamma_n = 1.35$ corresponds to the CAC 40 Index with ID number 5 and the EURO STOXX 50 Index with ID number 18 (both from Europe). After COVID-19, we have $\gamma_n \in [1.22, 1.72]$. The largest value of $\gamma_n = 1.72$ is for the Ibovespa Index with ID number 8 from Brazil and the S&P 500 market with ID number 16, while the smallest value, $\gamma_n = 1.22$, is for the Taiwan Weighted Index with ID number 9 from Taiwan, China. Moreover, the values of γ_n for three markets, including the DJI with ID number 3 from the USA, the JTOPI with ID number 13 from South Africa, and Brent crude oil with ID number 23, are independent of the disease COVID-19 (the difference is less than 0.04).

Before COVID-19, we have $\alpha_n \in [0.87, 1.93]$. The JTOPI with ID number 13 has the largest value of $\alpha_n = 1.93$. The IXIC with ID number 17 (NASDAQ Composite Index from the USA) has the smallest value of $\alpha_n = 0.87$. During COVID-19, we have $\alpha_n \in [0.56, 1.55]$. The S&P BSE Sensex 30 Index with ID number 10 from India has the largest value of $\alpha_n = 1.55$, and the smallest value of $\alpha_n = 0.56$ corresponds to the CAC 40 Index with ID number 5 from Europe. After COVID-19, we have $\alpha_n \in [0.53, 1.72]$. The largest value of $\alpha_n = 1.72$ comes from the CAC 40 Index with ID number 5 from Europe, while the smallest one, $\alpha_n = 0.53$, is from the Taiwan Weighted Index with ID number 9 from Taiwan, China. Moreover, the value of α_n for Brent crude oil with ID number 23 is independent of the disease COVID-19 (the difference is less than 0.13).

Before COVID-19, we have $\eta_n \in [0.48, 0.86]$. The EURO STOXX 50 Index with ID number 18 from Europe has the largest value of $\eta_n = 0.86$. The Ibovespa Index with ID number 8 from Brazil has the smallest value of $\eta_n = 0.48$. During COVID-19, we have $\eta_n \in [0.54, 0.79]$. The Hang Seng Index with ID number 2 from mainland China has the largest value of $\eta_n = 0.79$, while the smallest value of $\eta_n = 0.54$ corresponds to the gold spot price with ID number 24. After COVID-19, we have $\eta_n \in [0.45, 0.92]$. The largest value of $\eta_n = 0.92$ comes from the Taiwan Weighted Index with ID number 9 from Taiwan, China, while the smallest one, $\eta_n = 0.45$, comes from the RTS Index with ID number 12 from Russia. Moreover, the values of η_n for the NASDAQ Composite Index with ID number 17 from the USA and Brent crude oil with ID number 23 are independent of COVID-19 (the difference is less than 0.04).

In Table 2, in each column, i.e., the values for each specific exponent from the perspectives of different markets, the maximums and minimums are highlighted in red and blue, respectively. Interestingly, the maximums for γ_n and α_n and the minimums for η_n occur from the perspectives of the market sets with ID numbers $(8, 12, 16, 24)$, $(5, 10, 13)$, and $(8, 12, 24)$, which correspond to Russia, India, Brazil, South Africa, and the gold price, with the exception of ID number 5 (Europe) and ID number 16 (USA). The minimums for γ_n and α_n and the maximums for η_n occur from the perspectives of the market sets with ID numbers $(5, 9, 16, 18)$, $(5, 9, 17)$, and $(2, 9, 18)$, which correspond to the USA, Europe, and China (Taiwan and Hong Kong).

In Table 2, the rows where the exponent values before, during, and after COVID-19 remain almost unchanged are highlighted in gray. The similarity network from the perspective of the crude oil market, i.e., the Brent Europe crude oil prices, is independent of the COVID-19 pandemic.

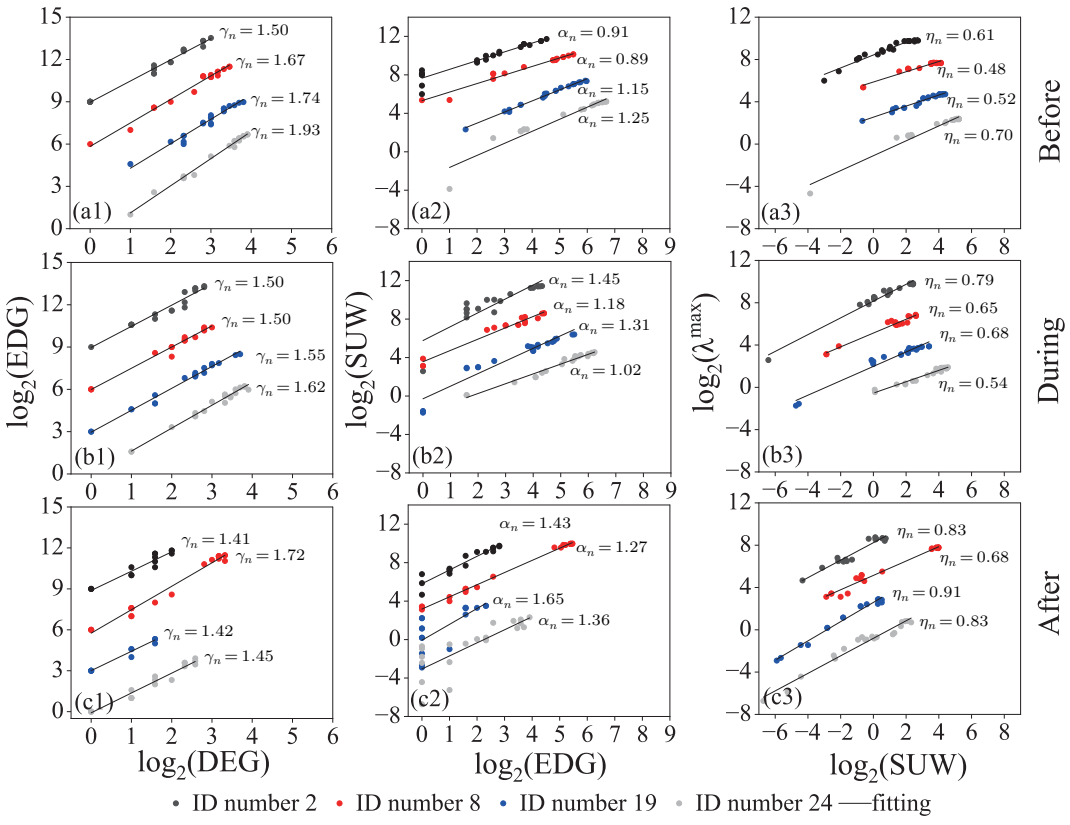


Fig. 6. Properties of the similarity networks from the perspectives of each market. The panels in the columns of $n \in [1,2,3]$ and the rows of $s \in [\mathrm{a},\mathrm{b},\mathrm{c}]$) refer to the relations EDG versus DEG, SUW versus EDG, and $\lambda^{\max}$ versus SUW before, during, and after COVID-19, respectively. As typical examples, the properties of similarity networks from the perspectives of the markets with ID numbers 2 (HSI from Mainland China), 8 (IBOV from Brazil), 19 (TASI from Saudi Arabia), and 24 (XAU/USD, the gold market) are shown. For visual convenience, the curves are shifted vertically.

4. Summary

Detecting correlation is a basic task in time series analysis and even in data-driven analysis. Current methods are designed from an objective perspective, i.e, the researcher tries to be outside the investigated system, adopts a set of measures that can extract exact and complete information for the agents, finds the relationships, and subsequently makes an objective decision. This kind of approach can answer questions such as 'how often', 'how many', and 'what is the relationship between variables'. However, in reality, the researcher is usually one of the agents in the system, participating in the formation and operation of the investigated system. The researcher has to design a set of metrics from their own specific behaviors, using which they construct a portrait of the system and make a decision from their own perspective, trying to answer questions such as 'how' and 'why'. In social science, this kind of investigation, which treats the researcher as an instrument, is called qualitative research; such research has provided plenty of new knowledge about social systems and subsequently deepened our understanding of them.

In this work, inspired by qualitative research, we propose a concept called ISP to reveal the correlations in a complex system from different perspectives, all of which form a multilayer portrait of the correlation. The procedure is first illustrated with the Lorenz system, the Rössler system, and their coupled system. Although the trajectory for each variable stores the precise dynamical information for the whole system, as guaranteed by Takens's theorem, our findings show that the behaviors of the trajectories for the variables may have significant differences that cannot be displayed by investigations in the literature. The ISP is then used to investigate a financial system composed of 22 stock markets distributed across the world, one gold market, and one crude oil market. The similarity networks constructed from the perspectives of the markets distributed in the USA, Europe, and China are homogeneous, and their topological structures are dominated by star patterns. The similarity networks constructed from the perspectives of the markets from Russia, Brazil, South Africa, and India are inhomogeneous, and their topological structures are dominated by cluster patterns.

In reality, people usually tend to (or have to) make decisions according to their findings and understanding to maximize their specific interests and realize their specific aims. A multilayer portrait constructed from different perspectives may provide us with a basis for exchanging ideas and thus for realizing effective communication with one another. Hence, our approach may find applications in a variety of problems in social, financial, ecological, and management systems, and even in technical systems with distributed infrastructures

where a central command system is absent.

Herein, we present a note on the mathematical and logical basis for the proposed framework. As mentioned in the introduction to the first section, qualitative research can not only avoid the requirements for the availability, completeness, and objectivity of data in quantitative research but also present us with perspective-dependent complexities for a complex system, providing us with a solid foundation for the efficient exchange of ideas and opinions. It accordingly attracts extensive attention and has made fruitful achievements in the research fields of sociology, psychology, and education. However, its development is accompanied by a persistent argument to the effect that it is subjective, which seems to be controversial, given the aim of current quantitative research. In this work, we try to present a framework that offers a balance between the two paradigms, i.e., one that places qualitative research on a quantitative foundation and introduces perspective-specific complexities into quantitative research.

The key idea is to precisely define the instrumental function of the researcher and realize it in a quantitative way. As an illustration of this idea, the time series of the researcher is decomposed into IMFs to represent its characteristics. The set of dominant characteristics is defined to be the 'sensors' of the instrument. By inputting the time series for a specific subsystem into the instrument, the sensors preserve (or filter out) the components whose characteristics match (or mismatch) their own, resulting in a state vector. From the state vectors of all the subsystems, the researcher calculates the distances between subsystems and constructs a distance network, i.e., a specific-researcher-dependent portrait of correlation.

Hence, the purpose of the expanded form in Eq. (5) is to map the subsystems' time series onto the multiple characteristics of the researcher, where the matching components are preserved and the other components are filtered out. The set of characteristics represented by the IMFs essentially acts as a 'filter'. Generally speaking, the IMFs in this filter are not orthogonal to each other, and the phase space spanned by them is incomplete. It should be emphasized that herein we are designing a specific-researcher-dependent filter that preserves components with matching characteristics rather than a complete orthogonal system that precisely represents the subsystems.

Actually, if we assume that the sets of IMFs constructed from the subsystems are all complete orthogonal systems, then all the researchers from the subsystems' perspectives can obtain complete and exact information for the whole system. Specifically, for a deterministic nonlinear dynamical system, because the manifolds for all the variables embedded in a high-dimensional phase space are equivalent to each other and to that for the whole system, the assumption implies that the phase spaces spanned by the variables' sets of IMFs are equivalent to each other, while the correlation structures of the system obtained by different researchers are equivalent, i.e., linear transformations can make them collapse together. The obtained correlations are subsequently specific-researcher-independent, i.e., they are trivial from the viewpoint of qualitative research. On the contrary, the non-equivalent and/or incomplete phase spaces spanning the sets of IMFs for different researchers (which may actually have different dimensions) may provide us with rich and varied information about the structure of correlation, i.e., the obtained correlation structures are specific-researcher-dependent. Hence, from the viewpoint of qualitative research, the nontrivial portrait of correlation comes from the non-equivalence between and/or incompleteness of the phase spaces spanned by the sets of IMFs for different researchers.

Appendix A

Herein, we present the coordinates for a total of 6 variables $x_1, y_1, z_1, x_2, y_2, z_2$ in the coupled chaotic system in the phase spaces spanned by the IMFs of x_1, y_1, z_1, x_2, z_2, respectively. These coordinates can provide us with a deep understanding of the corresponding similarity networks in Fig. 4. The coordinates in the phase space spanned by the IMFs of y_2 (taken to be the researcher) are given in Eqs. (22)–(24) in the main text.

$$V^{\cdot|x_1}(C=1) = \begin{pmatrix} 0.759 & 0.812 & 0.083 & -1.221 & -1.584 & -0.600 \\ 1.042 & -0.287 & 0.258 & 0.346 & 0.337 & 0.340 \end{pmatrix}, \tag{A1}$$

$$V^{\cdot|y_1}(C=1) = \begin{pmatrix} -0.228 & 1.141 & 0.288 & -0.096 & -0.183 & -0.167 \\ -0.176 & 1.159 & -1.397 & -1.775 & -1.253 & -1.197 \end{pmatrix}, \tag{A2}$$

$$V^{\cdot|z_1}(C=1) = \begin{pmatrix} -0.049 & -0.000 & 1.164 & -0.014 & -0.060 & 0.135 \\ 0.196 & 0.279 & 0.960 & 0.045 & 0.238 & -0.417 \\ -0.473 & -0.289 & 0.999 & -0.354 & -0.609 & 0.169 \\ 1.264 & 1.385 & 1.006 & 0.218 & -0.012 & 0.325 \\ 0.377 & -0.794 & 0.937 & -0.300 & -0.382 & -0.058 \\ 0.340 & -0.435 & 1.223 & 0.879 & 0.491 & 0.693 \end{pmatrix}, \tag{A3}$$

$$V^{\cdot|x_2}(C=1) = \begin{pmatrix} 0.570 & -0.060 & -0.267 & 1.232 & 1.110 & 0.259 \\ 0.530 & -0.654 & 0.155 & 0.900 & 0.753 & 0.363 \\ -0.192 & 0.004 & 0.127 & 1.028 & 0.908 & 0.494 \\ 0.059 & -0.081 & 0.084 & 0.969 & 0.835 & 0.261 \\ 0.050 & -0.076 & 0.041 & 1.188 & 1.070 & 0.395 \end{pmatrix}, \tag{A4}$$

$$V^{\cdot|z_2}(C=1) = \begin{pmatrix} -0.116 & 0.268 & 0.085 & 0.187 & -0.262 & 0.947 \\ 0.630 & -0.489 & 0.002 & 0.064 & 0.140 & 1.021 \\ 0.008 & -0.250 & 0.420 & 0.441 & 0.258 & 0.918 \\ -0.113 & -0.385 & 0.487 & 1.942 & 1.690 & 1.124 \end{pmatrix}, \tag{A5}$$

$$V^{\cdot|x_1}(C=3)$$
$$= \begin{pmatrix} 0.783 & 0.688 & 0.001 & -0.226 & -1.008 & -0.897 \\ 1.037 & -0.265 & 0.280 & 0.108 & 0.001 & 0.509 \end{pmatrix}, \quad \text{(A6)}$$
$$V^{\cdot|y_1}(C=3)$$
$$= \begin{pmatrix} -0.227 & 1.089 & 0.353 & -0.436 & -0.273 & -0.185 \\ -0.004 & 1.138 & -1.560 & 0.955 & 0.703 & -1.121 \end{pmatrix}, \quad \text{(A7)}$$
$$V^{\cdot|z_1}(C=3)$$
$$= \begin{pmatrix} -0.062 & -0.024 & 1.161 & 0.060 & -0.476 & 0.353 \\ 0.194 & 0.308 & 0.944 & 0.230 & 1.562 & -0.441 \\ -0.468 & -0.321 & 1.006 & -1.252 & -1.303 & -0.472 \\ 1.270 & 1.420 & 1.012 & -0.057 & -0.521 & 0.883 \\ 0.393 & -0.794 & 0.949 & -0.721 & -0.384 & -0.149 \\ 0.307 & -0.475 & 1.250 & -0.724 & -0.700 & 0.932 \end{pmatrix}, \quad \text{(A8)}$$
$$V^{\cdot|x_2}(C=3)$$
$$= \begin{pmatrix} -0.001 & 0.266 & -0.352 & 0.951 & 0.650 & 0.418 \\ 0.167 & -1.810 & -0.381 & 1.153 & 0.684 & 0.718 \\ -0.476 & 1.108 & -1.142 & 1.184 & 0.725 & 0.429 \end{pmatrix}, \quad \text{(A9)}$$
$$V^{\cdot|z_2}(C=3)$$
$$= \begin{pmatrix} -0.323 & 0.220 & -0.068 & 0.737 & -0.252 & 1.025 \\ 1.274 & -0.433 & 0.078 & 0.687 & 0.090 & 0.969 \\ 0.370 & -2.143 & 0.937 & -0.387 & -0.369 & 0.964 \\ -0.265 & 0.268 & 0.285 & -0.032 & -0.127 & 1.015 \end{pmatrix}, \quad \text{(A10)}$$
$$V^{\cdot|x_1}(C=8)$$
$$= \begin{pmatrix} 0.609 & 0.439 & 0.115 & -0.126 & -0.056 & -0.379 \\ 1.070 & -0.233 & 0.272 & 0.101 & -0.036 & 0.318 \end{pmatrix}, \quad \text{(A11)}$$
$$V^{\cdot|y_1}(C=8)$$
$$= \begin{pmatrix} -0.225 & 1.098 & 0.368 & -0.213 & -0.146 & -0.168 \\ 0.042 & 1.183 & -1.666 & 0.016 & 0.149 & -1.194 \end{pmatrix}, \quad \text{(A12)}$$
$$V^{\cdot|z_1}(C=8)$$
$$= \begin{pmatrix} -0.020 & 0.030 & 1.168 & -0.437 & 0.018 & -0.373 \\ 0.123 & 0.182 & 0.937 & 0.837 & -0.596 & 0.910 \\ -0.412 & -0.195 & 1.012 & -0.697 & 0.389 & -1.171 \\ 1.198 & 1.320 & 0.999 & -0.234 & -0.575 & 0.396 \\ 0.470 & -0.723 & 0.979 & -0.184 & 0.108 & -0.127 \\ 0.319 & -0.399 & 1.204 & 0.007 & -0.131 & 0.737 \end{pmatrix}, \quad \text{(A13)}$$
$$V^{\cdot|x_2}(C=8)$$
$$= \begin{pmatrix} -0.015 & 0.239 & 0.250 & 0.953 & 0.525 & 0.473 \\ 0.284 & -0.831 & -0.759 & 1.093 & 0.667 & 0.767 \end{pmatrix}, \quad \text{(A14)}$$
$$V^{\cdot|z_2}(C=8)$$
$$= \begin{pmatrix} -0.295 & 0.133 & -0.103 & 0.912 & -0.226 & 1.031 \\ 1.591 & -0.507 & -0.127 & 0.780 & 0.100 & 0.969 \\ -0.208 & -2.078 & 0.524 & 0.091 & 0.031 & 0.993 \\ -0.141 & 0.568 & 0.144 & 0.154 & 0.099 & 0.992 \end{pmatrix}. \quad \text{(A15)}$$

References

[1] Galton F 1888–1889 *Proc. R. Soc. Lond.* **45** 135
[2] de Abril I M, Yoshimoto J and Doya K 2018 *Neural Networks* **102** 120
[3] Peng C -K, Buldyrev S V, Havlin S, Simons M, Stanley H E and Goldberger A L 1994 *Phys. Rev. E* **49** 1685
[4] Scafetta N and Grigolini P 2002 *Phys. Rev. E* **66** 036130
[5] Podobnik B and Stanley H E 2008 *Phys. Rev. Lett.* **100** 084102
[6] Roulston M S 1999 *Phys. D* **125** 285
[7] Sugihara G, May R, Ye H, Hsieh C H, Deyle E, Fogarty M and Munch S 2012 *Science* **338** 496
[8] Bashan A, Bartsch R P, Kantelhardt J W, Havlin S and Ivanov P C 2012 *Nat. Commun.* **3** 702
[9] Schreiber T 2000 *Phys. Rev. Lett.* **85** 461
[10] Jolliffe I T 2002 *Principal Component Analysis*, 2nd edn. (New York: Springer-Verlag) p. 1
[11] Kotz S and Johnson N L 1992 *Breakthroughs in Statistics Volume II: Methodology and Distribution*(New York: Springer-Verlag) p. 162
[12] Yang X H, Liu W F, Liu W and Tao D C 2021 *IEEE Trans. Knowl. Data Eng.* **33** 2349
[13] Zhao Q K, Li S, Gu C G, Wang H Y and Yang H J 2025 *Chin. Phys. B* **34** 028702
[14] Wan H Y, Wang H Y, Gu C G and Yang H J 2025 *Nonlinear Dyn.* **113** 11455
[15] Ren H G, Yuan Q S, Semba S, Weng T F, Gu C G and Yang H J 2020 *Phys. Lett. A* **384** 126781
[16] Yan S, Gu C G and Yang H J 2024 *Physica A* **637** 129534
[17] Yan S, Gu C G and Yang H J 2025 *Commun. Nonlinear Sci. Numer. Simulat.* **140** 108344
[18] Yuan Q S, Zhang J, Wang H Y, Gu C G and Yang H J 2023 *Chaos Solitons & Fractals* **172** 113589
[19] Kyzar E J and Denfield G H 2023 *Mol. Psychiatry* **28** 10
[20] Perry B L, Pescosolido B A and Borgatti S P 2018 *Egocentric Network Analysis: Foundations, Methods, and Models* (Cambridge: Cambridge University Press) p. 1
[21] Yang S 2024 *Social Network Analysis in Action: Basic Methods and Applications* (Cham: Springer) p. 1
[22] Scott J and Carrington P J 2011 *The SAGE Handbook of Social Network Analysis* (London: SAGE Publications Ltd) p. 404
[23] Crossley N and Edwards G 2016 *Sociol. Res. Online* **21** 13
[24] Traxler A L, do Amaral C M D, Henderson C, LaForge E, Hatcher C, Swirtz M and Barthelemy R 2024 *Phys. Rev. Phys. Educ. Res.* **20** 020132
[25] Huang N E, Shen Z, Long S R, Wu M C, Shih H H, Zheng Q, Yen N C, Tung C C and Liu H H 1998 *Proc. R. Soc. Lond. A* **454** 903
[26] Wu Z H and Huang N E 2009 *Adv. Adapt. Data Anal.* **1** 1
[27] Lorenz E N 1963 *J. Atmos. Sci.* **20** 130
[28] Rössler O E 1976 *Phys. Lett. A* **57** 397
[29] Le van Quyen M, Martinerie J, Adam C and Varela F J 1999 *Phys. D* **127** 250
[30] https://cn.investing.com. Downloaded on November 03, 2025.
[31] https://fred.stlouisfed.org/series/DCOILBRENTEU. Downloaded on November 03, 2025.
[32] https://www.who.int/europe/emergencies/situations/covid-19
[33] Huang C L, Wang Y M, Li X W, Ren L L, Zhao J P and Hu Y 2020 *Lancet* **395** 497